Potential Temperature and Potential Vorticity Inversion: Complementary Approaches

JOSEPH EGGER

Meteorologisches Institut, Universität München, Munich, Germany

KLAUS-PETER HOINKA

Institut für Physik der Atmosphäre, DLR, Oberpfaffenhofen, Germany

(Manuscript received 14 April 2010, in final form 21 June 2010)

ABSTRACT

Given the distribution of one atmospheric variable, that of nearly all others can be derived in balanced flow. In particular, potential vorticity inversion (PVI) selects potential vorticity (PV) to derive pressure, winds, and potential temperature θ. Potential temperature inversion (PTI) starts from available θ fields to derive pressure, winds, and PV. While PVI has been applied extensively, PTI has hardly been used as a research tool although the related technical steps are well known and simpler than those needed in PVI. Two idealized examples of PTI and PVI are compared. The 40-yr European Centre for Medium-Range Weather Forecasts (ECMWF) Re-Analysis (ERA-40) datasets are used to determine typical anomalies of PV and θ in the North Atlantic storm-track region. Statistical forms of PVI and PTI are applied to these anomalies. The inversions are equivalent but the results of PTI are generally easier to understand than those of PVI. The issues of attribution and piecewise inversion are discussed.

1. Introduction

Many aspects of large-scale fluid dynamics can be understood within the framework of ''potential vorticity (PV) thinking'' (Hoskins et al. 1985, hereafter HMR), where PV plays a central role as a materially conserved quantity in the absence of friction and heating. It is sufficient according to this concept to know the distribution of PV at a certain moment as well as balance and boundary conditions to derive most other variables by PV inversion (PVI) (e.g., Vallis 1996; Arbogast et al. 2008). In particular, pieces of PV are inverted (PPVI; e.g., Davis 1992) because ''a unique influence on the rest of the atmosphere'' (Bishop and Thorpe 1994) is attributed to them. It is customary in PVI to say that PV anomalies induce velocity fields at some distance (e.g., HMR). It is this dynamic interpretation of PV and PVI that provided much of the motivation for applying PVI and PPVI so widely (e.g., Bleck 1990). The inversion procedures tend to be fairly complicated when nonlinearities have to be included (Davis and Emanuel 1991).

At the moment PVI appears to be the dominant inversion method used in diagnostics of atmospheric dynamics (e.g., Smy and Scott 2009). We have to keep in mind, however, that all atmospheric variables are related in balanced flow. Given one of them, nearly all the others can be derived. A priori, none of the standard variables is more important than others. For example, pressure p provides a case in point. Potential temperature θ follows from p by applying the hydrostatic relation. Geostrophic winds are then also available and with that PV after some additional calculations. The result is at least as realistic as that obtained via PVI, since PV does not contain more information than p or θ in balanced flow. One may argue that pressure is not conserved. This speaks, of course, in favor of PV. A forecast of PV is possible on the basis of the winds derived from the master variable PV (Warn et al. 1995). However, θ is also conserved in the absence of diabatic heating and thus has the same rank as PV with respect to conservation properties (see also Vallis 1996). Inversion of potential temperature (PTI) is straightforward in a hydrostatic atmosphere (see section 2 for technical details) and yields pressure and then also PV, where the term ''inversion'' is understood in a broad sense. For example, satellite radiometer measurements are said to be inverted to yield vertical temperature profiles (e.g., Andrews et al. 1987). Various versions of PTI were the

Corresponding author address: Joseph Egger, Meteorological Institute, University of Munich, Theresienstr. 37, 80333 Munich, Germany.
E-mail: j.egger@lrz.uni-muenchen.de

DOI: 10.1175/2010JAS3532.1

backbone of data analysis in the early days of numerical weather forecasting when almost only radiosonde observations were available (Hollingsworth 1986). Constructing geopotential heights, winds, and PV from satellite-derived temperatures is another example. It appears to be a new idea, however, that PTI is simply the inverse of PVI and might therefore be as helpful as PVI for an understanding of atmospheric dynamics.

Thus, θ and PV appear to be equivalent with respect to inversion. This equivalence is obvious in the quasigeostrophic framework where PV is

$$q_g = \nabla^2\psi + f + f_o^2(\overline{\rho})^{-1}\frac{\partial}{\partial z}\left(\overline{N}^{-2}\overline{\rho}\frac{\partial}{\partial z}\psi\right) \qquad (1.1)$$

in standard notation and θ is replaced by $\partial\psi/\partial z$. To perform PTI, one has to know the ''temperature'' $\partial\psi/\partial z$ in the fluid and ψ at, say, the upper boundary. It is then straightforward to evaluate ψ and, finally, q_g. Similarly, PVI yields ψ after solving an elliptic equation and $\partial\psi/\partial z$ if q_g is known in the fluid as well as, say, ψ at the boundaries. Thus PVI reverts PTI and PTI reverts PVI. However, q_g is conserved while the omega equation must be solved to predict temperature. This advantage of PVI is lost when we turn to the primitive equations where θ is conserved and to a good approximation

$$q = \rho^{-1}(\zeta + f)\frac{\partial\theta}{\partial z} \qquad (1.2)$$

with relative vorticity ζ.

An intercomparison of both methods may begin with the simple statement that PTI is superior from a technical point of view. There is little doubt that PVI is the most complicated method to derive the variables of balanced flow from a single one. It has been demonstrated, however, again and again that PVI is nevertheless helpful in providing insights into flow dynamics. For example, HMR discuss barotropic and baroclinic instability in the light of PVI, and Harnik et al. (2008) elucidate shear instability along these lines. In contrast, PTI has hardly been invoked to explain dynamic mechanisms. Baroclinic instability in the Eady model is a rare example. Here, we will discuss first two idealized cases to recall the steps of PTI and to demonstrate the prognostic capacity of the method. PVI will be applied in parallel.

We turn to observations in the second part of this paper, keeping in mind that the atmosphere is generally close to a balanced state. That means that PVI and/or PTI need not be carried out mathematically. Given, for example, ''global'' observations of θ we know that the result of PTI must be close to the observations of pressure and winds provided a sufficiently realistic balance condition has been chosen. The situation is different if the inversions are carried out with respect to anomalies of PV or θ restricted to a domain D_1. This is the situation in PPVI when $q' = 0$ is assumed in D_2 outside D_1 and $D = D_1 + D_2$ is the total flow domain. This choice implies that anomalies θ' will be found in D_2. The concept of piecewise PTI (PPTI) is introduced here in parallel with $\theta' = 0$ in D_2 but we will also consider briefly a version of PPTI with $q' = 0$ in D_2. In general, the results of PPVI (PPTI) cannot be taken from observations and the inversions have to be carried out mathematically. However, we may derive the typical structure of localized PV (θ) anomalies from observations. For example, point correlation maps provide accurate information on the relation of atmospheric fields such as pressure or temperature to a localized anomaly of θ or PV. We do not have to invert these anomalies explicitly because the data reveal the result. This statistical approach is inspired by Hakim and Torn (2008, hereafter HT), Hakim (2008), and Gombos and Hansen (2008). However, PPTI appears to imply that we can also attribute to θ anomalies an influence on the rest of the atmosphere.

2. Potential temperature inversion: Idealized examples

We will discuss in this section two idealized examples of PTI and relate them to PVI.

a. Single θ anomaly

The first idealized case of PTI to be discussed is based on an axisymmetric localized θ anomaly

$$\theta' = -\tilde{\theta}F(z)\sin(2\pi z/H)\cos^2\alpha, \qquad (2.1)$$

with $\alpha = \pi r/2r_1$ in a stably stratified f-plane atmosphere of 20-km depth at rest. The anomaly (2.1) is restricted to the cylinder $0 \le z \le H$ of radius $r = r_1$ centered at $r = 0$, where $\tilde{\theta}$ is constant and the prime denotes a perturbation with respect to the background. A warm anomaly is located above a cold one (Fig. 1a). We have here also an idealized example of PPTI since the θ anomaly is restricted to the cylinder D_1 and $\theta' = 0$ elsewhere. The hydrostatic equation

$$\frac{\partial}{\partial z}(p/p_{oo})^{R/c_p} = -g/(c_p\theta) \qquad (2.2)$$

in standard notation with constant p_{oo} has to be integrated downward from the top level where the pressure perturbation p' is assumed to vanish. The function F in (2.1) is chosen such that $p' = 0$ at the surface. With $p' = 0$ at $z = H$ and $z = 0$, pressure anomalies are negative

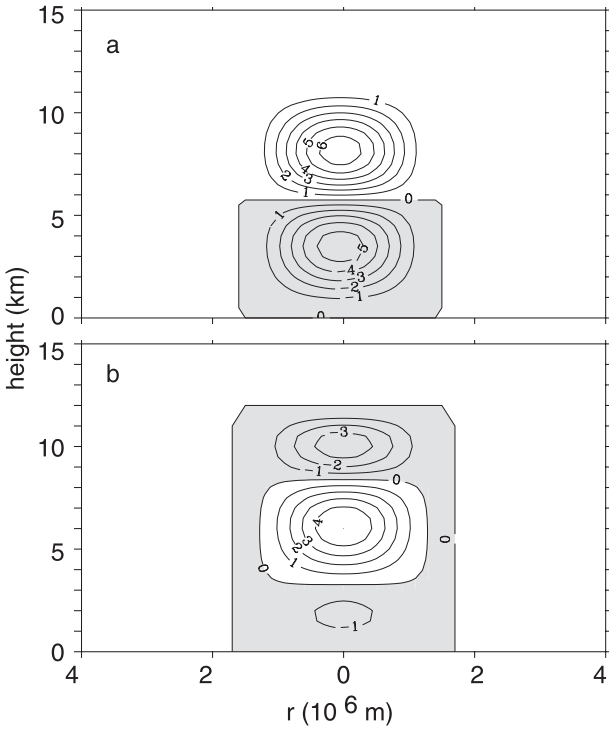

FIG. 1. (a) Illustration of PTI for an axisymmetric θ anomaly (K) of radius $r_1 = 1.5 \times 10^6$ m and depth $H = 12$ km and (b) the related PV anomaly (PVU); negative values shaded.

within the cylinder (not shown) and $p' = 0$ outside. The square in (2.1) ensures a vanishing of the geostrophic winds at $r = r_1$. Their rotation is cyclonic within the cylinder, of course. The geostrophic vorticity

$$\zeta_g' = (\overline{\rho} f_o)^{-1} \nabla^2 p' \tag{2.3}$$

is localized as well with

$$\int_o^{r_1} \zeta_g' r \, dr = 0. \tag{2.4}$$

Since $\zeta_g' > 0$ close to the origin, there must be a ring of negative vorticity around the positive values in the center. More realistic balance conditions (e.g., Charney 1955) could have been used as well but the simple geostrophic balance is preferable in our illustrative examples. Finally, the PV anomaly is

$$q' \sim (\overline{\rho})^{-1} \left(\zeta_g' \frac{\partial}{\partial z} \overline{\theta} + f_o \frac{\partial \theta'}{\partial z} \right), \tag{2.5}$$

where only the most important terms are given.

The second term in (2.5) dominates the PV field in Fig. 1b where a positive anomaly is sandwiched between two negative ones. The switch of the sign of ζ_g' in the horizontal as implied by (2.4) is visible in Fig. 1b only near $z = H/2$. All in all, a qualitative PTI is carried out easily in this case.

We support this qualitative inversion by simplified calculations where we assume a Boussinesq atmosphere with constant background variables. Thus, pressure

$$p' = \overline{\rho} \tilde{\theta} g H (2\pi \overline{\theta})^{-1} [\cos(2\pi z/H) - 1] \cos^2 \alpha \tag{2.6}$$

follows from (2.1) with $F(z) = 1$ and from the hydrostatic Boussinesq relation

$$\frac{\partial p'}{\partial z} = \overline{\rho} g \theta' / \overline{\theta}. \tag{2.7}$$

Pressure is negative everywhere in the cylinder and vanishes at $z = 0$ and $z = H$. Inserting (2.6) and (2.1) in (2.5) gives

$$q' = -\frac{d\overline{\theta}}{dz} \tilde{\theta} g H (2 r_1 \overline{\theta} \overline{\rho} f_o)^{-1} [(\cos\alpha \, \sin\alpha)/r + \pi/(2 r_1)(\cos^2\alpha - \sin^2\alpha)]$$
$$[\cos(2\pi z/H) - 1] - 2\pi f_o \tilde{\theta} H^{-1} \cos(2\pi z/H) \cos^2\alpha, \tag{2.8}$$

where the first term represents the contribution of the vorticity [see (2.5)] and the second one that of the temperature gradient. The vorticity is positive at $r = 0$ and negative at $r = r_1$ where there is a jump of vorticity with $\zeta_g' = 0$ outside the cylinder.

PVI requires us to derive the θ anomaly in Fig. 1a from the PV anomaly in Fig. 1b. The actual calculations would be nonlinear because (2.5) contains a nonlinear term in complete form but we can assume here that the necessary iterations result in a sufficiently accurate approximation to Fig. 1a. The PV anomalies in Fig. 1b are restricted to the cylinder D_1 and $q' = 0$ in D_2. Following the examples in HMR and Bishop and Thorpe (1994), we expect to find temperature anomalies in the horizontal for $r > r_1$ and a penetration (HMR) above the PV anomaly. However, there are no θ anomalies outside the cylinder D_1, so a qualitative PVI based on standard ideas is impossible.

The simplified mathematical PVI requires us to solve

$$q' = (\overline{\rho})^{-2} \left[\frac{d\overline{\theta}}{dz} (f_o r)^{-1} \frac{\partial}{\partial r} \left(r \frac{\partial p'}{\partial r} \right) + f_o \overline{\theta} g^{-1} \frac{\partial^2 p'}{\partial z^2} \right], \tag{2.9}$$

where q' is given by (2.8) in the cylinder and $q' = 0$ outside. One has to find the solution (2.6) either by intuition or by mathematical methods. Thus, the first step of PVI is not simple. The θ anomaly follows then from (2.7).

The above example demonstrates that q' can be derived from θ' and vice versa in balanced flow. However, one would not claim that q' can be attributed to θ'.

b. Interactions

As stated above, it is an advantage both of PVI and PTI that predictions of flow evolution can be made using the winds resulting from the inversion and invoking the conservation of PV and/or θ. As an example of "θ thinking," a qualitative prediction of vortex interaction will be made on the basis of an initial θ field.

We prescribe two separate anomalies of potential temperature in a double periodic domain D, which of course also represent anomalies of potential vorticity. Interaction of θ anomalies is automatically also vortex interaction. The anomalies are embedded in an f-plane atmosphere at rest of 20-km depth that is composed of a troposphere with a constant lapse rate of 5×10^{-3} K m^{-1} and an isothermal stratosphere above a tropopause at a height $H_T = 12$ km. Two circular warm anomalies A_1 and A_2 are prescribed with maxima at locations Z_1 and Z_2, respectively (see Fig. 2a). The potential temperature anomalies θ' have the same horizontal structure as in (2.1) with radius $r_1 = 1000$ km while the vertical profile is sinusoidal. Anomaly A_1 is located in the lower troposphere ($z < H_S = 6$ km) whereas A_2 is defined in the upper troposphere ($z > H_S$).

A zonal cross section of the potential temperature anomalies at the "latitude" $y = 0$ of maximum temperature perturbations is shown in Fig. 2a. The horizontal distance of both anomalies is chosen such that A_2 extends partly above A_1. The corresponding pressure anomalies result from an integration of (2.2) with pressure anomaly $p' = 0$ on top of the domain.

It follows that negative pressure anomalies are found in and below the positive potential temperature anomalies. The geostrophic circulation related to A_1 and A_2 is thus cyclonic but (2.4) is satisfied at every level. As before, there are positive vorticity anomalies near and below the centers of the θ anomalies surrounded by rings of negative vorticity. The geostrophic wind at Z_1 is northerly and vanishes at Z_2.

The PV anomalies related to the θ anomalies are displayed in Fig. 2b. The PV anomaly underneath the center of A_2 is positive because of the cyclonic circulation there. Its amplitude is growing upward near $z = H_S$ because of the increase of the potential temperature with height in the lower part of A_2. Rings of negative PV surround the positive centers of A_1 and A_2. Moreover, $q' < 0$ on top of A_1 and A_2. A qualitative estimate of Fig. 2b is easy on the basis of Fig. 2a.

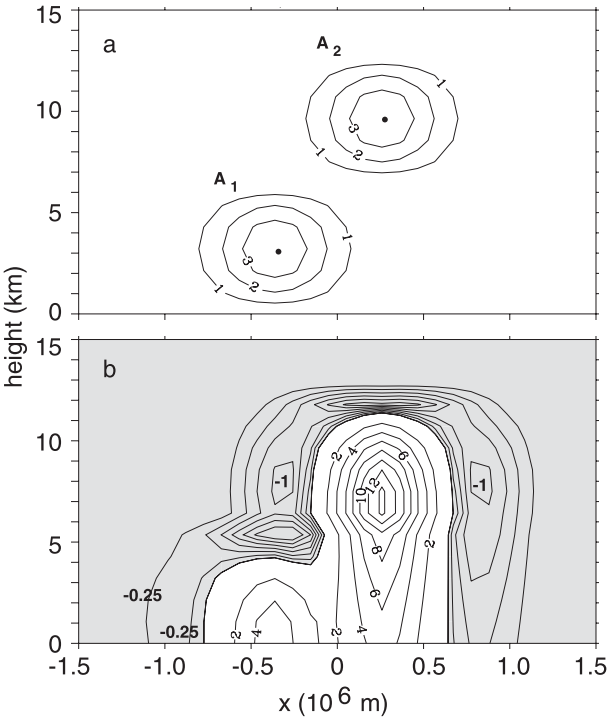

FIG. 2. Initial anomalies of (a) potential temperature (contour interval = 0.5 K) and (b) potential vorticity (PVU) in the plane $y = 0$ in the interaction case with two warm anomalies (cyclonic vortices) discussed in the text; the dots mark the locations of the temperature maxima of A_1 and A_2; contour interval is 0.25 PVU for negative and 2.0 PVU for positive values; negative values are shaded.

Now let us try to predict the motion of the anomalies on the basis of PV thinking and of the analogous θ thinking. Note that θ thinking in terms of geostrophic transports predicts a cyclonic rotation of A_1 around A_2 while A_2 does not move.

Qualitative PV thinking has to face the complicated PV field in Fig. 2b. Again, one would expect to find temperature anomalies above and around the PV centers. Since these do not exist, a qualitative form of PVI is hardly possible. One would not guess that there are no winds at Z_2. A crude prediction could be based on the idea that there are mainly two positive PV anomalies that would rotate around each other. Since the PV anomaly of A_2 is about 3 times stronger than that related to A_1, one would expect the low-level anomaly to move faster than the upper-level one. This prediction neglects (2.4) and the rings of negative PV in Fig. 2b.

These qualitative predictions have been tested by running a quasigeostrophic model for one day. The result corroborates the estimates of θ thinking in that A_1 rotates indeed around A_2 while the upper-level anomaly hardly moves at all (not shown).

The idealized cases demonstrate that θ thinking can be superior to PV thinking. Of course, examples could be designed as well where PV thinking is more appropriate (e.g., HMR). In particular, θ thinking cannot be applied in barotropic fluids.

3. Statistical inversions

a. Methods

So far, θ anomalies have been prescribed in order to demonstrate the basic ideas and techniques of PTI. As a next step we have to look at observed anomalies of θ and PV to investigate the merits of PTI and PVI. As stated above we choose a statistical approach that is related to the concept of a statistical PVI introduced by HT (see also Hakim 2008 and Gombos and Hansen 2008). These authors deal with ensembles of weather forecasts to analyze the role of PV anomalies (ensemble statistical analysis). The basic idea is to assume a linear relationship

$$p'_k = \sum_i L_{ki} q'_i \tag{3.1}$$

between the gridpoint values p'_k of, say, pressure and q'_i of potential vorticity anomalies, where the indices k and i run over all grid points. The matrix $\mathbf{L}$ would be essentially the inverse of the Laplacian in quasigeostrophic flow but HT estimate $\mathbf{L}$ from the data. Thus,

$$C(q_j, p_k) = \sum_i L_{ki} C(q_j, q_i) \tag{3.2}$$

(j runs over all points) is the proper set of equations for the coefficients L_{ki} provided the covariances in (3.2) are available where $C(b, s)$ is the covariance of variable b and variable s. Note that any set of variables can be inserted in (3.1). For example, we may replace q'_i in (3.1) by θ'_i and p'_i by q'_k to have an example of statistical PTI.

HT refine their approach by considering specific patches of PV. That makes good sense in the ensemble statistical analysis where a specific synoptic situation is investigated. However, such specific patterns are not available a priori in climatological data. Instead, the observations are needed to define typical anomalies. A standard method is to apply the point correlation approach (e.g., Blackmon et al. 1984; Lim and Wallace 1991; Chang 1993). A correlation point P is selected as well as a key variable b with $b = \hat{b}$ at P. The first step consists in evaluating covariances $C(\hat{b}, s)$ of $\hat{b}$ and other variables s defined throughout the atmosphere. Thus, $C(\hat{\theta}, \theta)$ provides information on the typical structure of θ anomalies centered at the key point and $C(\hat{q}, q)$ describes the typical PV anomaly. The choice of gridpoint values $\hat{b}$ for the covariance analysis is convenient but we could just as well use other more complicated combinations of gridpoint values such as spatial means. It has been decided to restrict the analysis to the simplest case that is known to provide localized anomalies.

Our analysis is based on 40-yr European Centre for Medium-Range Weather Forecasts (ECMWF) Re-Analysis (ERA-40) data for the winters [December–February (DJF)] 1958–2001. Time series of θ and p are used at constant height surfaces $z = z_i$ with a distance of $Dz = 2000$ m except for the lowest two ($z_1 = 1000$ m; $z_2 = 2000$ m; $z_3 = 4000$ m, etc). The interpolation to height coordinates is linear. All time series are exposed to the high-pass filter of Blackmon and Lau (1980) that excludes fluctuations with periods >10 days. Covariances are calculated at grid points where a typical grid box covers an area of 2.25° × 2.25° in longitude and latitude and has a depth of Dz.

As pointed out by HT, we do not have to carry out the inversion procedures mathematically because the result is known from the climatological data analysis. For example, statistical PVI starts from the covariances $C(\hat{q}, q_i)$ and wishes to obtain $C(\hat{q}, p_k)$. However, the covariances $C(\hat{q}, p_k)$ are known from observations and we have just to interpret the relation of both fields. It is advantageous for the understanding of the results if quasilinear relations are assumed. For example, (2.2) is a nonlinear relation but anomalies are relatively small and we can therefore invoke the linearized version

$$\frac{\partial}{\partial z}[C(\hat{\theta}, p)/\overline{p}^{c_p/c_v}] = C(\hat{\theta}, \theta) g p_{oo}^{R/c_p}/(R\overline{\theta}^{-2}) \tag{3.3}$$

of (2.2) in interpretations of the results.

In principle, any point can be chosen as a correlation point, but the computational effort is quite large even for one point. It has been decided to select just two points located in a dynamically active storm-track region. The first point P_1 (47.25°N, 45.0°W; $z = 8$ km) is located in the upper troposphere of the North Atlantic storm track while P_2 (47.25°N, 40.5°W; $z = 2$ km) is slightly east of P_1 in the lower troposphere.

In what follows we will present normalized covariance functions $C(\hat{b}, s)/\sigma_b$, where σ_b is the standard deviation of $\hat{b}$. Such covariances may also be called regressions.

b. Statistical PVI

The normalized covariances $C(\hat{q}_1, q)$ at $z = 8$ km as displayed in Fig. 3b contain a "circle" of positive correlations of radius ~750 km and domains with negative values in the east and west, the western one being slightly stronger. The anomalies are essentially restricted to the Atlantic sector so that the statistical analysis yields localized structures as required by PPVI. The covariances outside this sector are quite small and may not pass a

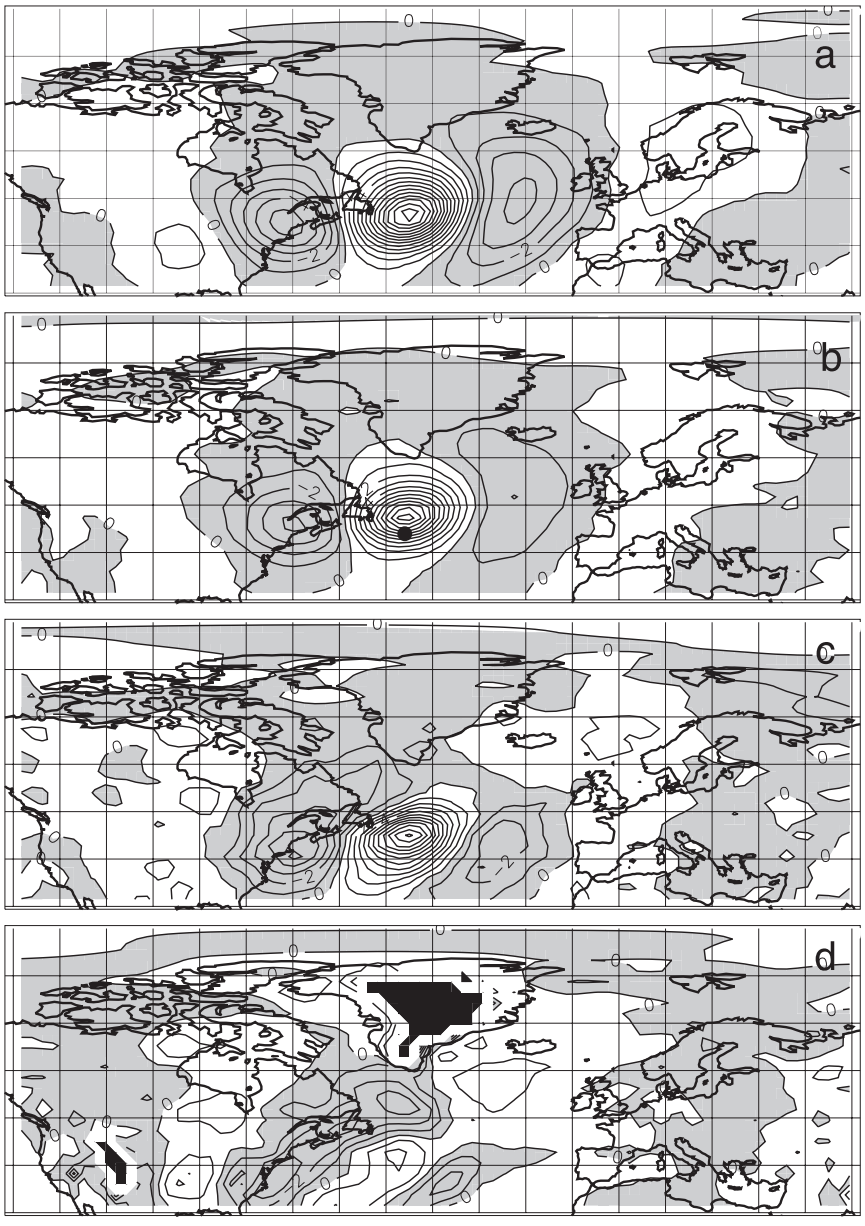

FIG. 3. Normalized covariance $C(\hat{q}_1, q)$ of $\hat{q}_1$ and PV for the correlation point P_1: (a) z = 12 km (contour interval = 0.1 PVU); (b) z = 8 km (0.1 PVU); (c) z = 4 km (0.01 PVU); (d) z = 2 km (0.01 PVU). The dot in (b) marks the location of P_1 at z = 8 km; the dot is shifted slightly southward for the maximum to become better visible. Negative values are shaded; areas of no data are dark (ERA-40; DJF).

significance test. Covariances are quite similar at z = 12 km but with a stronger minimum in the east (Fig. 3a). The relative importance of the western minimum grows with decreasing height but amplitudes decrease (Figs. 3c,d). All in all, we have in Fig. 3 the shape of a typical PV anomaly in the North Atlantic storm track, with large covariances in the upper troposphere and lower stratosphere, where the anomaly is centered, and small amplitudes close to the ground. The vertical extent of the anomaly is at least 10 km. We have not been able to find point correlation maps of PV in the literature but the structure of the central positive PV column in Fig. 3 is, for example, similar to that of Hakim (2000), who searched for coherent 500-hPa vorticity maxima.

To make a guess of the associated pressure and θ fields, we invoke the standard picture of isolated PV anomalies as in HMR and Bishop and Thorpe (1994), where isentropes are lowered (raised) above (below)

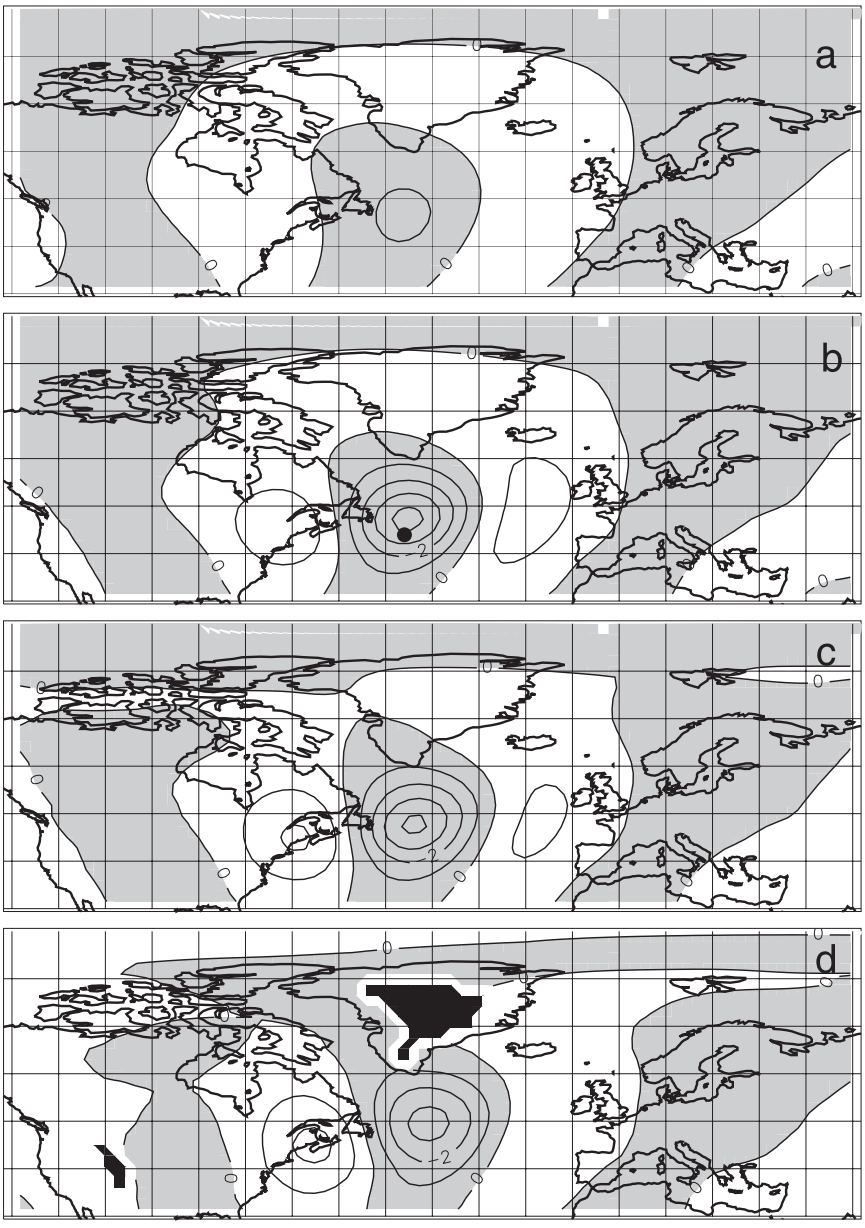

FIG. 4. As in Fig. 3, but for the normalized covariance $C(\hat{q}_1, p)$ of $\hat{q}_1$ and pressure (contour interval = 1 hPa).

a PV anomaly. One expects a pressure minimum at the center of the positive anomaly. The pressure patterns in Fig. 4 support these ideas reasonably well for each of the PV columns in Fig. 3 but the extrema are not very distinct. Potential temperatures are negative below P_1 and positive above where a somewhat surprising dipole forms (Fig. 5). The scale of the θ anomalies is the same as that of the PV anomalies. There are no indications of a far field in Figs. 4 and 5. This is about as far as we can go with qualitative PPVI.

It helps in the interpretation of Figs. 3–5 to take the reverse route as in PPTI. Given the radius $r_1 \sim 750$ km of the anomalies in Figs. 3–5, it follows from (2.3) that

$$\zeta' \sim -p'/(\overline{\rho} f_o r_1^2), \tag{3.4}$$

where the covariance symbols are omitted. A PV anomaly of 0.1 PV units (PVU, where 1 PVU $= 10^{-6}$ m^2 s^{-1} K kg^{-1}) can be generated by a pressure perturbation

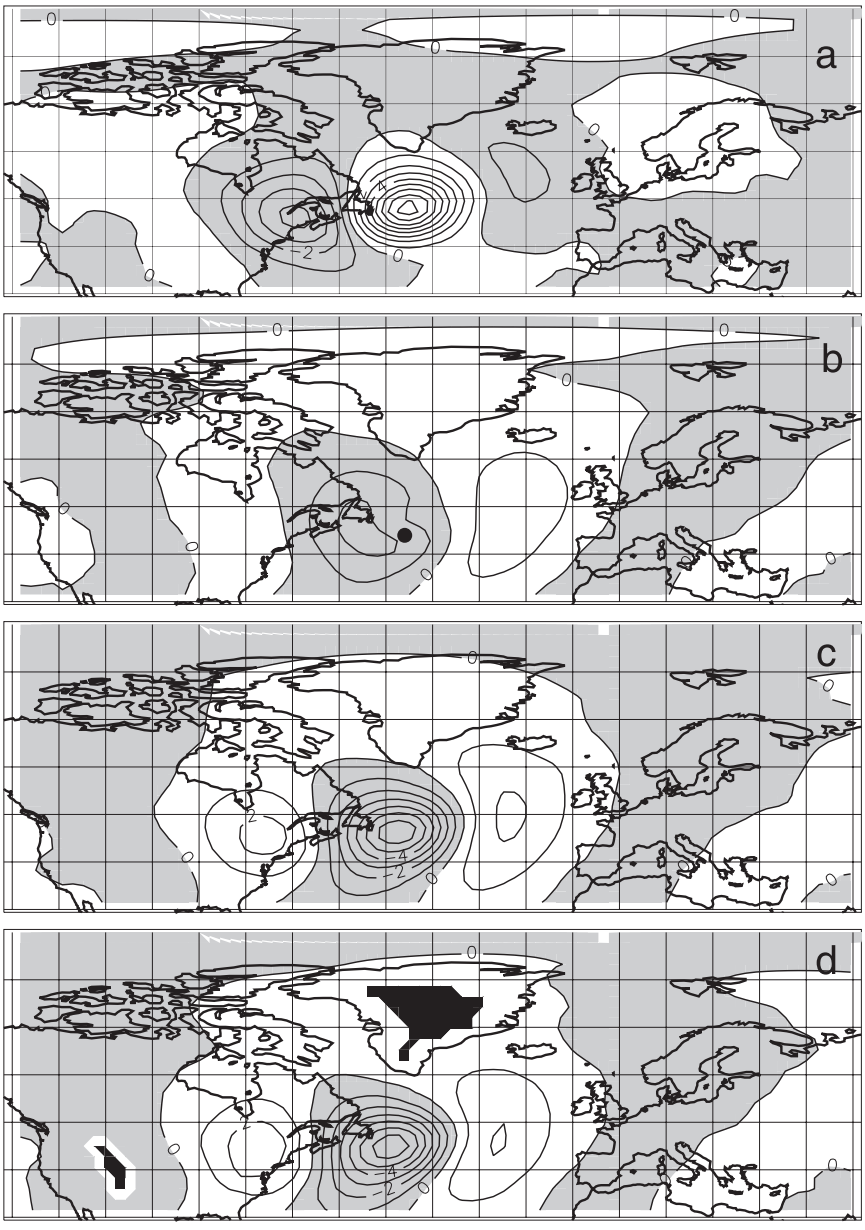

FIG. 5. As in Fig. 3, but for the normalized covariance $C(\hat{q}_1, \theta)$ of $\hat{q}_1$ and potential temperature (contour interval = 0.5 K).

$$\delta p = -10^{-7}\overline{\rho}^2 f_o r_1^2 \left(\frac{d\overline{\theta}}{dz}\right)^{-1} \sim -2 \times 10^3 \overline{\rho}^2 \qquad (3.5)$$

in pascals [see (2.5)], while a separate θ difference

$$\Delta\theta' = 2\overline{\rho} \qquad (3.6)$$

in kelvins is needed over a depth $Dz = 2000$ m for the same effect. In practice, pressure and θ are not independent, of course. The estimates (3.5) and (3.6), however, give a feeling for relative contributions. Since q' almost vanishes in Fig. 3d, it follows that the pressure perturbation $\delta p \sim -3$ hPa there must be balanced by a small vertical temperature decrease of ~0.3 K, which is close to the limits of our resolution. On the other hand, the large PV anomaly of ~1.2 PVU in Fig. 3a is supported by a pressure contribution of only ~0.3 PVU, so the temperature gradient is a main factor in generating the PV anomaly.

Geostrophic winds transport PV and/or θ if the isobars form angles with the isolines of PV or the isentropes. The isobars in Fig. 4 are fairly parallel to the PV isolines

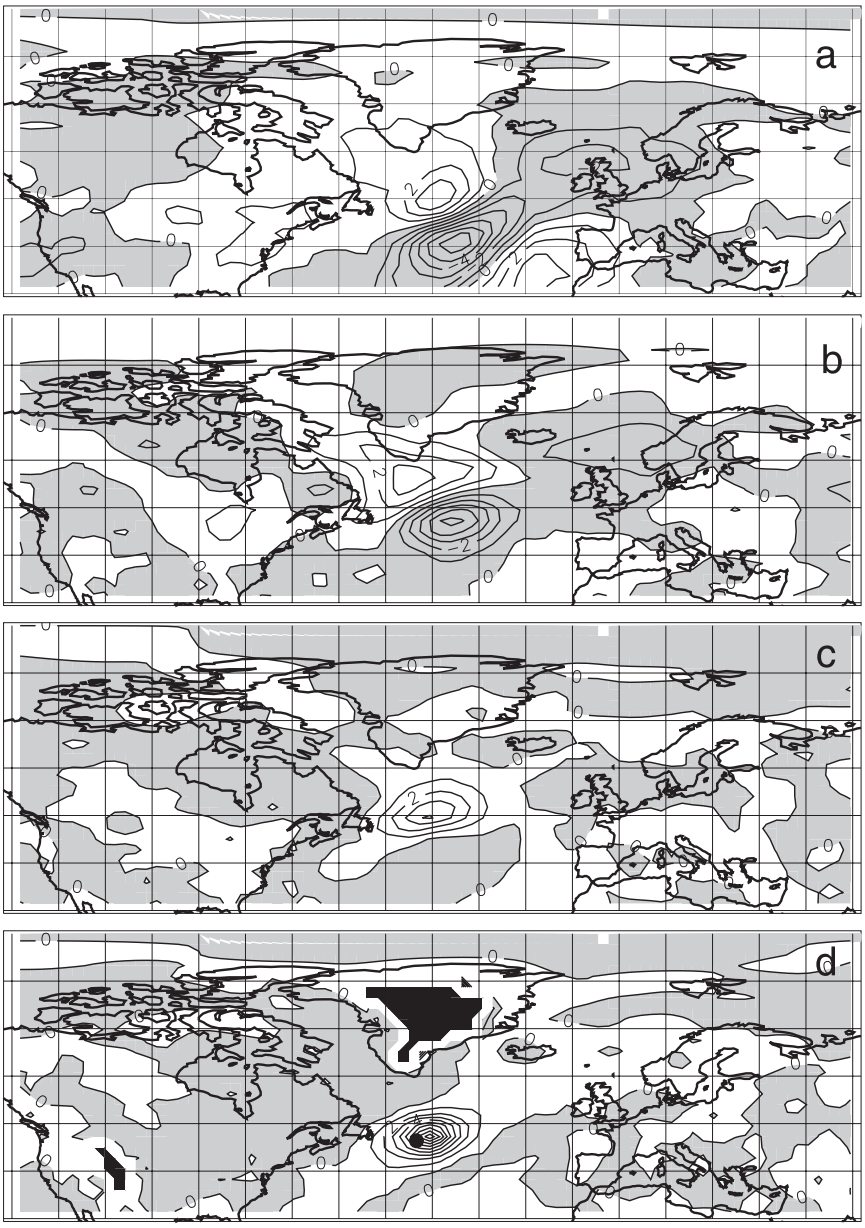

FIG. 6. Normalized covariance $C(\hat{q}_2, q)$ in of $\hat{q}_2$ and PV for P_2: (a) $z = 12$ km (contour interval = 0.04 PVU); (b) $z = 8$ km (0.04 PVU); (c) $z = 4$ km (0.02 PVU); (d) $z = 2$ km (0.02 PVU). The dot in (d) marks the location of P_2 at $z = 2$ km. Negative values are shaded; areas of no data are dark (ERA-40; DJF).

so that no transport of PV by geostrophic winds is to be expected. On the other hand, the negative θ anomaly in Fig. 5d is exposed to northerlies. Thus, we have here indications of an amplification, a rather unexpected result for a statistical analysis.

The typical PV anomaly centered at P_2 (Fig. 6) differs greatly from that in Fig. 3. There is a column of positive covariances extending from $z = 2$ km into the stratosphere with a slight northward tilt. Amplitudes decrease weakly with height. The greater axis of the ''ellipse'' at $z = 2$ km has a length of ~500 km and there are no upstream and downstream minima. However, a fairly large patch of negative covariances is found at $z = 8$ km and $z = 12$ km slightly southeast of the location of P_2, so that there is a strong dipole aloft. The PV anomalies are fairly localized in the lower troposphere but more extended at the upper levels. In particular, there is a secondary minimum over Great Britain and a maximum over the

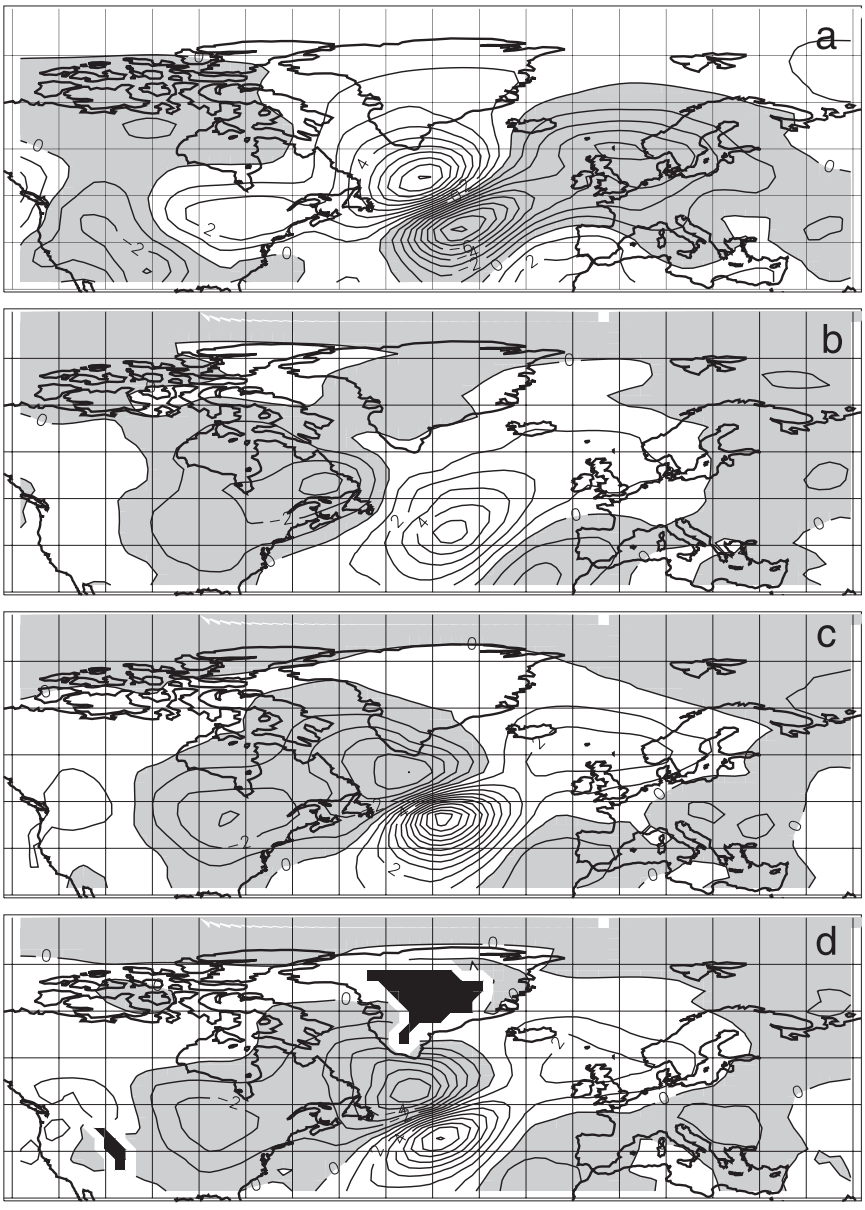

FIG. 7. As in Fig. 6, but for the normalized covariance $C(\hat{q}_2, \theta)$ of $\hat{q}_2$ and potential temperature θ (contour interval = 0.1).

Mediterranean at $z = 12$ km. To save space, the covariances $C(\hat{q}_2, p)$ are omitted and we turn to $C(\hat{q}_2, \theta)$ in Fig. 7. Dipoles are found at all levels with a switch of the sign between Figs. 7a and 7b. This time, the standard scheme is less helpful. It is true that θ anomalies are large and positive in the midtroposphere above P_2, but it is hard to explain the strong dipole structure of the θ fields in Figs. 7c and 7d. Note also that the θ anomalies are even less localized as the PV structures. The isolated PV maximum in Fig. 6d is supported by the positive gradient of θ' found there but it is open why the negative θ anomalies in the northwest are not reflected in the PV field.

c. *Statistical PTI*

The normalized covariance $C(\hat{\theta}_1, \theta)$ is displayed in Fig. 8. There is an almost circular domain of ~2000-km radius of positive covariances near P_1 (Fig. 8b) with adjoining domains of rather small negative values in the east and west. This structure extends down to the lowest level. There is a switch of sign higher up so that a rather cold anomaly is located above P_1 (Fig. 8a). We may also

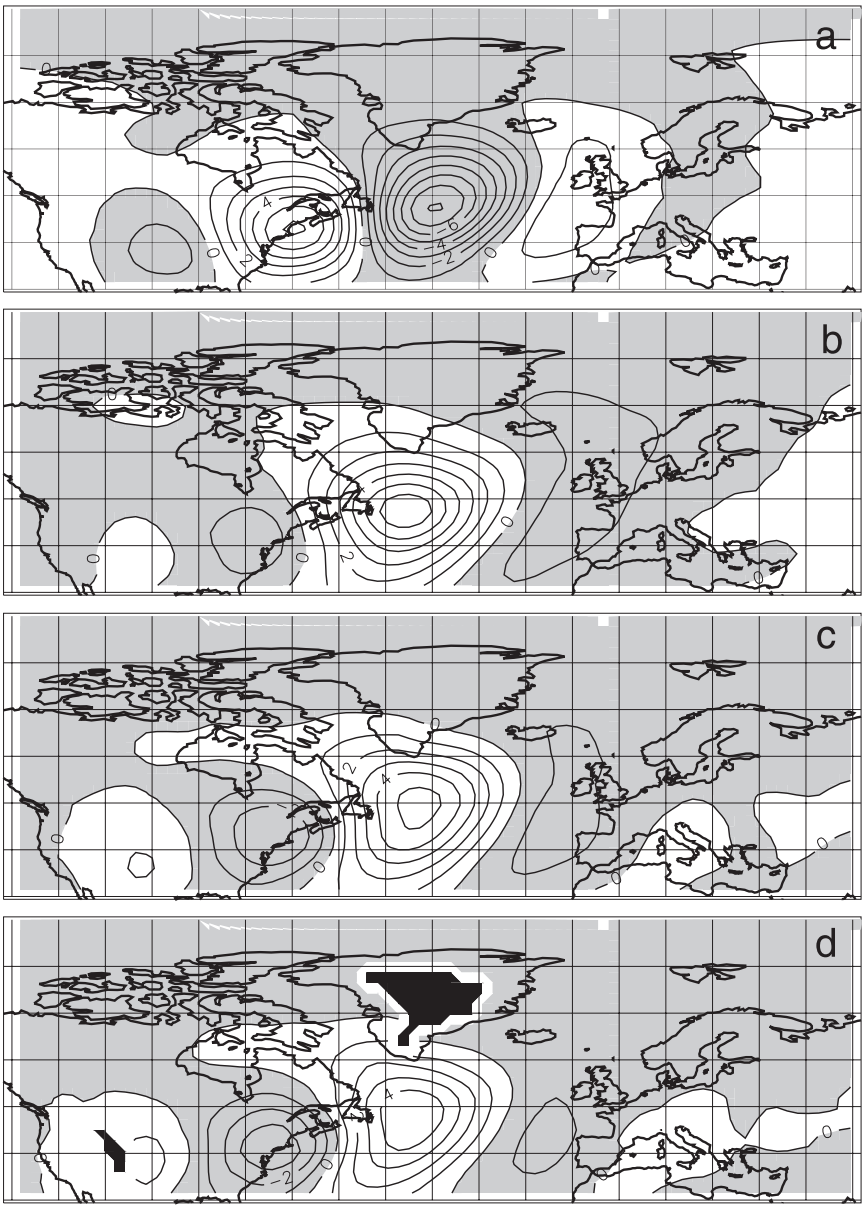

FIG. 8. As in Fig. 3, but for the normalized covariance $C(\hat{\theta}_1, \theta)$ of $\hat{\theta}_1$ and potential temperature (contour interval = 0.5 K).

say that the warm column tilts westward in the upper troposphere as do the cold ones.

To apply the hydrostatic relation, we have to accept the pressure distribution at 12 km as kind of an upper boundary condition (Fig. 9a). The pressure covariances are fairly small at $z = 12$ km with high pressure above P_1. There is indeed pressure increase (decrease) in warm (cold) areas if we proceed downward (Fig. 9). Thus, there is a strong low at $z = 2$ km underneath the column of cold air west of P_1 and a weak high east of the low. The PV field in Fig. 10 exhibits a rather strong negative center above P_1. Amplitudes go down quickly with decreasing height. The contribution by the pressure field to PV is reduced as compared to (3.5) because r_1 is larger, while (3.1) is unaltered. The vertical gradient of θ', however, is quite small and positive in Fig. 8 except between $z = 8$ km and $z = 12$ km. Thus, the positive PV anomalies below P_1 as well as the strong dipole at $z = 12$ km can be explained mainly by looking at the θ field. However, the negative PV center in Fig. 10b may be due to the pressure contribution but better vertical resolution would be needed to understand this pattern.

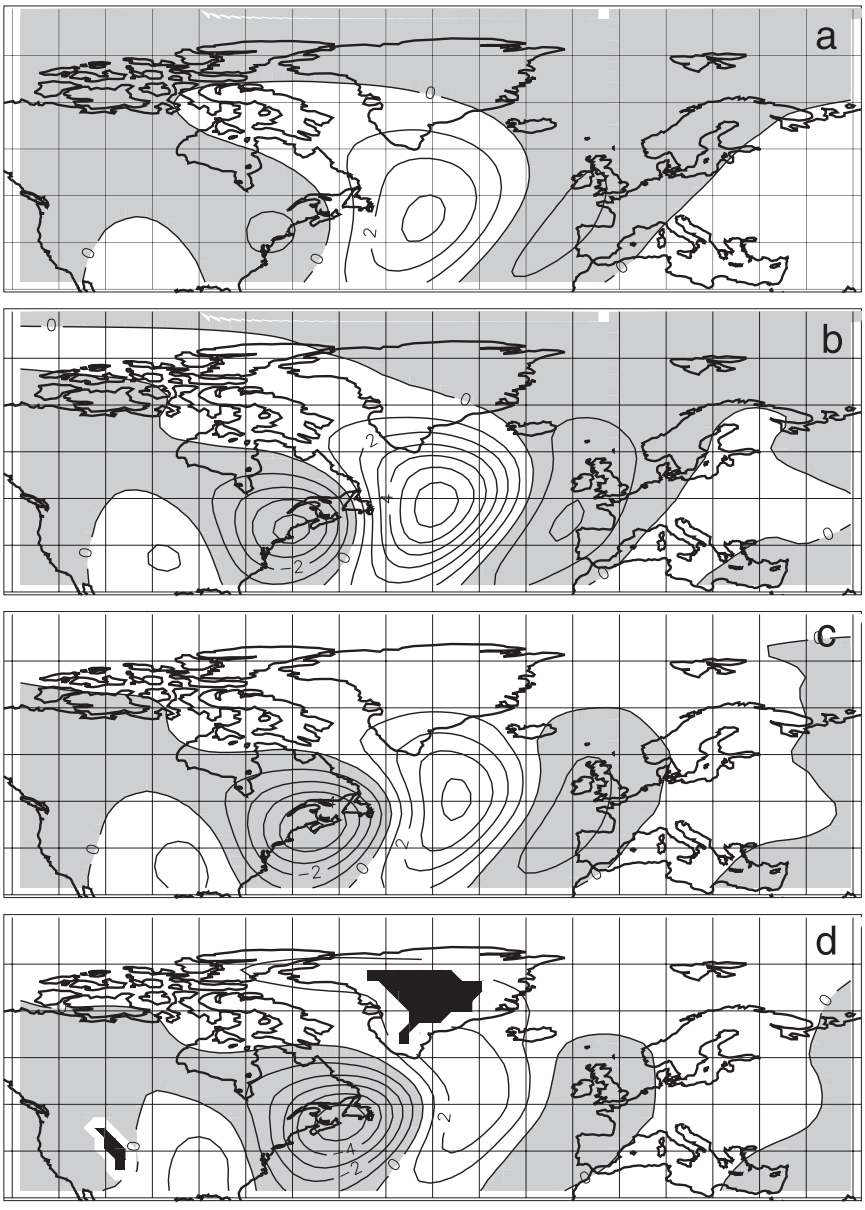

FIG. 9. As in Fig. 3, but for the normalized covariance $C(\hat{\theta}_1, p)$ of $\hat{\theta}_1$ and pressure (contour interval = 0.5 hPa).

Isobars and isentropes are not well aligned at z = 8 km (Figs. 8b and 9b). For example, there are geostrophic southerlies at P_1, which implies a damping of the θ anomaly. The center of the low in Fig. 9b is located slightly west of the PV minimum, which is therefore exposed to positive advection of background PV so that there is also a damping influence.

The typical θ anomaly centered at P_2 (Fig. 11) consists as in Fig. 8 of a column of positive anomalies above z = 2 km and a strong negative center in the stratosphere. Obviously Figs. 8 and 11 are quite similar. There appears to be just one type of θ anomaly, at least in the region of P_1 and P_2. This similarity implies that the PV patterns in Fig. 12 are also similar to those in Fig. 10, as is indeed the case. This is a further demonstration of the utility of PTI.

4. Discussion and conclusions

Both PVI and PTI exploit the notion of a balanced state of the atmosphere. Given one variable all others can be derived (except moisture), but θ and PV are prominent choices because they are conserved. The inversion

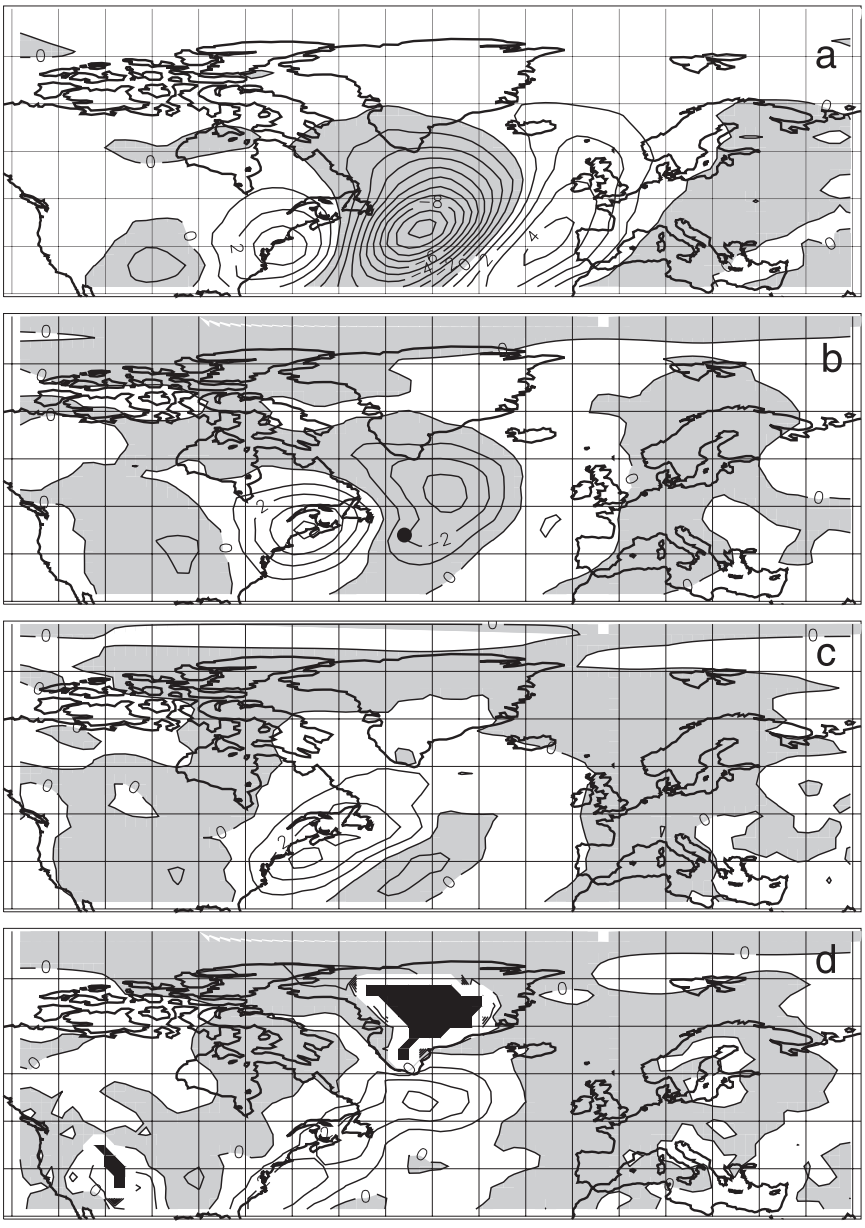

FIG. 10. As in Fig. 3, but for the normalized covariance $C(\hat{\theta}_1, q)$ of $\hat{\theta}_1$ and PV. Contour intervals are 0.1 PVU in (a),(b) and 0.02 PVU in (c),(d).

helps us to understand the dynamics of the atmosphere and to elucidate the structure of pressure and PV associated with a θ anomaly, for example. In turn, PVI inverts PTI. These statements are almost self-evident if ''global'' observations are available. An inversion does not even have to be carried out. This view does not hold when we turn to piecewise inversion, which has to be performed mathematically, at least in general. PPVI and PPTI differ because the former assumes $q' = 0$ outside the anomaly domain D_1 while PPTI is free to choose $\theta' = 0$ or $q' = 0$ in D_2. It is clear that there will be in general a far field in the latter case just as in PPVI. Moreover, it can be shown that PPVI and PPTI give the same quasigeostrophic solution in the case dealt with by Bishop and Thorpe (1994), where D_1 is a sphere with constant q'_g in PPVI, or with a prescribed temperature gradient corresponding to this flow state in PPTI. All this suggests that both methods yield similar results but a detailed comparison is beyond the scope of this paper. The inverted flows are essentially restricted to the atmospheric column enclosing D_1 if $\theta' = 0$ in D_2 is assumed in PPTI. There is no far field.

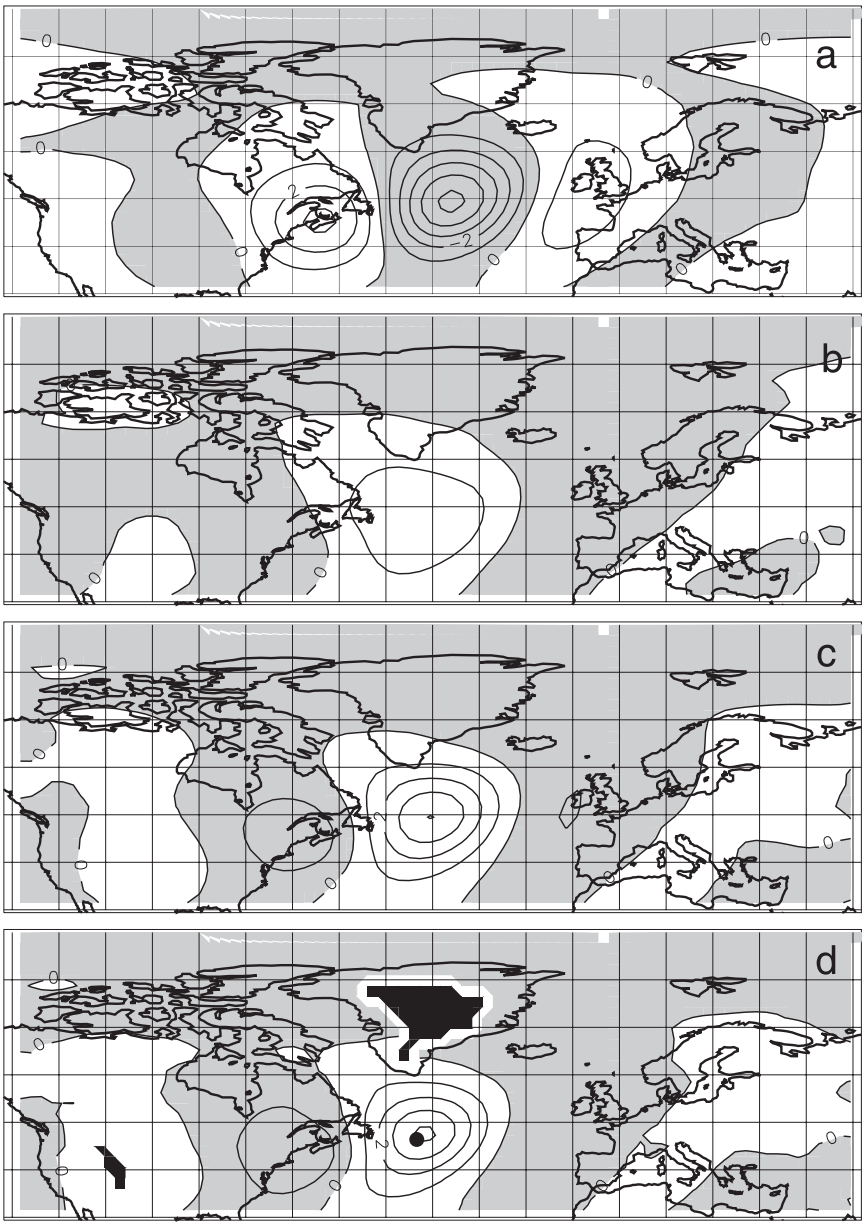

FIG. 11. As in Fig. 6, but for the normalized covariance $C(\hat{\theta}_2, \theta)$ of $\hat{\theta}_2$ and potential temperature (contour interval = 1.0 K).

Piecewise inversions search for the flow fields in balance with a selected anomaly. The observed flows are then compared with those obtained via inversion. Good agreement indicates that the balanced flow structures supporting this anomaly are close to those observed.

The idealized examples in section 2 were designed such that $q' = 0$ and $\theta' = 0$ outside the atmospheric columns enclosing the θ anomalies. Moreover, interaction of vortices has been predicted using PTI. It has been found in both cases that PTI is easier to apply and more helpful than PVI. The first steps of PTI, namely imposing the hydrostatic rule and evaluating geostrophic vorticity, are fairly simple. It is only the last step where qualitative assessment becomes difficult because the relative contributions of vorticity and temperature gradient to PV have to be estimated. It is the first step that is difficult in PVI. This made it almost impossible to apply PV thinking to Figs. 1b and 2b. Of course, PTI is easier to perform mathematically than PVI.

The main part of the paper is devoted to statistical inversions where the anomalies are defined by point correlations but where a mathematical inversion is not

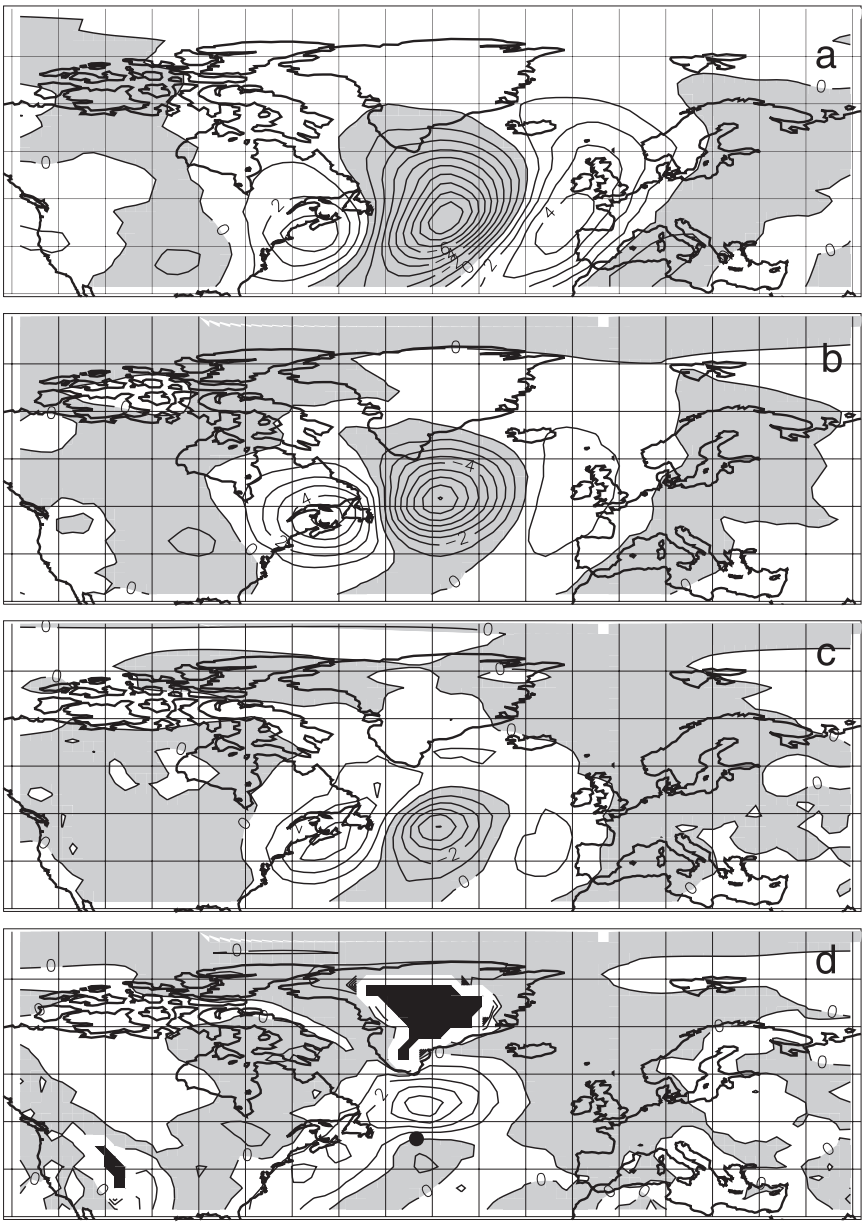

FIG. 12. As in Fig. 6, but for the normalized covariance $C(\hat{\theta}_2, q)$ of $\hat{\theta}_2$ and PV. Contour intervals are 0.1 PVU in (a),(b) and 0.02 PVU in (c),(d).

necessary because the result is contained in the observations. Two points in the North Atlantic storm-track region are chosen for the analysis and both PVI and PTI are carried out. This way we obtain the structure of atmospheric fields associated with typical PV and θ anomalies in the upper as well as in the lower troposphere. A qualitative derivation of the pressure and vorticity distributions from the θ anomaly is not difficult in PTI, but that of PV is more problematic. Qualitative PVI is moderately successful. It is a key result that the statistical PV anomalies are not associated with a far field of pressure and θ. Thus, the statistical inversions are also examples of PPVI and PPTI where the method selects also the anomaly area D_1 and where $q' \sim 0$ and $\theta' \sim 0$ outside D_1.

HMR argued in favor of PV thinking that PV anomalies tend to be more distinct and concentrated than, say, height fields. The statistical PV anomalies in Fig. 3 have a somewhat smaller horizontal scale than the θ anomalies in Fig. 8 and are somewhat better concentrated in the vertical. On the other hand, the low-level PV anomaly in Fig. 6 is highly distinct horizontally but has

a rather complex structure in the vertical. Thus, our point correlation maps do not favor one method.

As for attribution, it would be a strange claim that the θ anomalies in Figs. 8 and 11 have an impact on the rest of the atmosphere. The PV anomalies in Figs. 10 and 12 are just in balance with the θ anomalies. Of course, the same is true for the PV anomalies in Figs. 3 and 6.

Attempts have been made to test the nonlinearity of our results by conducting statistical analyses for situations with strong positive (negative) deviations where $\hat{\theta}$ must be larger (less) than the standard deviation σ_θ ($-\sigma_\theta$), but the outcome was fairly similar to what has been found here.

There are some significance problems in Hakim (2008) and Gombos and Hansen (2008) because relatively few forecasts are available. On the other hand, the ERA series contains so many analyses that we do not have to worry about significance of the basic structures in our figures.

Acknowledgments. Valuable comments by the referees helped to improve the paper.

REFERENCES

Andrews, D., J. Holton, and C. Leovy, 1987: *Middle Atmosphere Dynamics*. Academic Press, 489 pp.

Arbogast, P., K. Maynard, and F. Crepin, 2008: Ertel potential vorticity inversion using a digital filter initialization method. *Quart. J. Roy. Meteor. Soc.,* **134,** 1287–1296.

Bishop, C., and A. Thorpe, 1994: Potential vorticity and the electrostatic analogy: Quasi-geostrophic theory. *Quart. J. Roy. Meteor. Soc.,* **120,** 713–731.

Blackmon, M., and N.-C. Lau, 1980: Regional characteristics of the Northern Hemisphere wintertime circulation: A comparison of the simulation of a GFDL general circulation model with observations. *J. Atmos. Sci.,* **37,** 497–514.

——, Y. Lee, and J. Wallace, 1984: Horizontal structure of 500-mb height fluctuations with long, intermediate, and short time scales. *J. Atmos. Sci.,* **41,** 961–980.

Bleck, R., 1990: Depiction of upper/lower vortex interaction associated with extratropical cyclogenesis. *Mon. Wea. Rev.,* **118,** 573–585.

Chang, E. K. M., 1993: Downstream development of baroclinic waves as inferred from regression analysis. *J. Atmos. Sci.,* **50,** 2038–2053.

Charney, J., 1955: The use of the primitive equations of motion in numerical prediction. *Tellus,* **7,** 22–26.

Davis, C., 1992: Piecewise potential vorticity inversion. *J. Atmos. Sci.,* **49,** 1397–1411.

——, and K. Emanuel, 1991: Potential vorticity diagnostics of cyclogenesis. *Mon. Wea. Rev.,* **119,** 1929–1953.

Gombos, D., and J. Hansen, 2008: Potential vorticity regression and its relationship to dynamical piecewise inversion. *Mon. Wea. Rev.,* **136,** 2668–2682.

Hakim, G., 2000: Climatology of coherent structures on the extratropical tropopause. *Mon. Wea. Rev.,* **128,** 385–406.

——, 2008: A probabilistic theory for balance dynamics. *J. Atmos. Sci.,* **65,** 2949–2960.

——, and R. Torn, 2008: Ensemble synoptic analysis. *Synoptic–Dynamic Meteorology and Weather Analysis and Forecasting: A Tribute to Fred Sanders, Meteor. Monogr.,* No. 55, Amer. Meteor. Soc., 147–161.

Harnik, N., E. Heifietz, O. Umurhan, and F. Lott, 2008: A buoyancy–vorticity wave interaction approach to stratified shear flow. *J. Atmos. Sci.,* **65,** 2615–2630.

Hollingsworth, A., 1986: Objective analysis for numerical weather prediction. *Short- and Medium-Range Numerical Weather Prediction,* T. Matsumo, Ed., Meteorological Society of Japan, 11–60.

Hoskins, B., M. McIntyre, and A. Robertson, 1985: On the use and significance of isentropic potential vorticity maps. *Quart. J. Roy. Meteor. Soc.,* **111,** 877–946.

Lim, G., and J. Wallace, 1991: Structure and evolution of baroclinic waves as inferred from regression analysis. *J. Atmos. Sci.,* **48,** 1718–1732.

Smy, L., and R. Scott, 2009: The influence of stratospheric potential vorticity on baroclinic instability. *Quart. J. Roy. Meteor. Soc.,* **135,** 1637–1683.

Vallis, G., 1996: Potential vorticity inversion and balance equations of motion for rotating and stratified flows. *Quart. J. Roy. Meteor. Soc.,* **122,** 291–322.

Warn, R., O. Bokhove, T. Shepherd, and G. Vallis, 1995: Rossby number expansion, slaving principles, and balance dynamics. *Quart. J. Roy. Meteor. Soc.,* **121,** 723–739.